nature neuroscience

BRIEF COMMUNICATION

https://doi.org/10.1038/s41593-019-0556-3

Corrected: Author Correction

Dopamine metabolism by a monoamine oxidase mitochondrial shuttle activates the electron transport chain

Steven M. Graves[1], Zhong Xie[1], Kristen A. Stout[1], Enrico Zampese[1], Lena F. Burbulla[2], Jean C. Shih[3], Jyothisri Kondapalli[1], Tommaso Patriarchi[4], Lin Tian[4], Lars Brichta[5], Paul Greengard[5], Dimitri Krainc[2], Paul T. Schumacker[6] and D. James Surmeier[1]*

Monoamine oxidase (MAO) metabolizes cytosolic dopamine (DA), thereby limiting auto-oxidation, but is also thought to generate cytosolic hydrogen peroxide (H_2O_2). We show that MAO metabolism of DA does not increase cytosolic H_2O_2 but leads to mitochondrial electron transport chain (ETC) activity. This is dependent upon MAO anchoring to the outer mitochondrial membrane and shuttling electrons through the intermembrane space to support the bioenergetic demands of phasic DA release.

MAOs are oxidoreductases that deaminate catecholamines. In dopaminergic axons, released DA is taken up from the extracellular space, where it is recycled into vesicles or degraded by MAO. The biological rationale for cytosolic DA metabolism is unknown. One hypothesis is that MAO limits the generation of damaging quinones by DA auto-oxidation in the cytosol[1]. However, it is also currently thought that the electrons generated by MAO activity are transferred to molecular oxygen, resulting in the generation of cytosolic H_2O_2 that could damage proteins and lipids, particularly in axons where DA release and recycling are prominent[2,3].

To investigate this puzzling scenario, genetically encoded H_2O_2-sensitive optical thiol redox sensors[4] were expressed in subcellular compartments of dopaminergic neurons and pharmacological tools were used to acutely drive DA metabolism by MAO. First, a viral vector carrying an expression construct for a cytosolic redox-sensitive variant of green fluorescent protein (cyto-roGFP) was injected into the substantia nigra pars compacta (SNc) of mice. After infection, cyto-roGFP expression was evident throughout dopaminergic cell bodies, dendrites and axons (Extended Data Fig. 1a). Ex vivo brain slices were prepared, and two-photon laser scanning microscopy (2PLSM) was used to measure the thiol redox status of SNc dopaminergic neurons, which is altered by H_2O_2 and/or quinone generation. Unexpectedly, acute bath application of methamphetamine (10 µM; applied for 10–20 min), which increases cytosolic DA by disrupting vesicular monoamine transporters (VMATs)[5,6], failed to increase cytosolic oxidation in axons (the primary DA release site) or cell bodies (Extended Data Fig. 1f,g). The DA precursor levodopa (L-dopa) (100 µM; applied for >30 min), which elevates cytosolic DA by increasing synthesis[7], also had no measurable effect on cytosolic oxidation in this time frame (Extended Data Fig. 1f,h).

Although acutely increasing cytosolic DA did not affect cytosolic redox status, it increased axonal mitochondrial matrix thiol oxidation measured with a variant of roGFP that was targeted to the mitochondrial matrix (mito-roGFP) (Fig. 1a and Extended Data Fig. 1b). This effect on mitochondria was robust in axons (Fig. 1b–e), a region where DA is released and content is known to be high, but was absent in the cell body (Extended Data Fig. 2a). Reserpine treatment of mice (5 mg kg^{-1} once daily for 5 d), which depletes vesicular DA, prevented the mitochondrial redox effects of methamphetamine (Fig. 1f). Compounds that block the plasma membrane DA transporter, but do not inhibit VMATs (i.e., cocaine and methylphenidate), had no effect on the mitochondrial matrix redox status (Extended Data Fig. 2b).

Why might elevations in axonal DA increase mitochondrial, but not cytosolic, oxidant stress? MAO is anchored to the outer mitochondrial membrane, so it is possible that electrons arising from the metabolism of DA are not directly transferred to oxygen but are instead shuttled through the intermembrane space to the ETC. In this way, DA metabolism by MAO could contribute to the inner membrane potential, which is used to produce ATP.

As a first step toward testing this hypothesis, the type of MAO expressed by SNc dopaminergic neurons was determined. In agreement with work in human dopaminergic neurons[8], bacTRAP profiling of mRNA in mouse SNc dopaminergic neurons detected both *Maoa* and *Maob* mRNAs, with *Maoa* mRNA being the more abundant (19.76 ± 0.54 reads per kilobase per million for *Maoa* versus 4.49 ± 0.48 reads per kilobase per million for *Maob*; mean from $n = 6$ mice). When brain slices were pre-incubated with the MAO-B inhibitor rasagiline, the effects of elevating cytosolic DA on mitochondrial oxidation were attenuated (Fig. 1c,e). The MAO-A inhibitor clorgyline also diminished the mitochondrial redox effects of increasing cytosolic DA (Extended Data Fig. 2c). Neither rasagiline nor clorgyline altered basal mitochondrial matrix redox status, presumably reflecting low basal MAO activity in axons of ex vivo brain slices (Extended Data Fig. 2d). However, acutely elevating cytosolic DA in the presence of rasagiline caused the cytosolic thiol oxidation status to increase (Extended Data Fig. 1g,h), suggesting that, when MAO is inhibited, DA is auto-oxidized.

[1]Department of Physiology, Feinberg School of Medicine, Northwestern University, Chicago, IL, USA. [2]Department of Neurology, Feinberg School of Medicine, Northwestern University, Chicago, IL, USA. [3]Department of Pharmacology and Pharmaceutical Sciences, School of Pharmacy, University of Southern California, Los Angeles, CA, USA. [4]Department of Biochemistry and Molecular Medicine, School of Medicine, University of California-Davis Davis, Davis, CA, USA. [5]Laboratory of Molecular and Cellular Neuroscience, Rockefeller University, New York, NY, USA. [6]Department of Pediatrics, Feinberg School of Medicine, Northwestern University, Chicago, IL, USA. *e-mail: j-surmeier@northwestern.edu

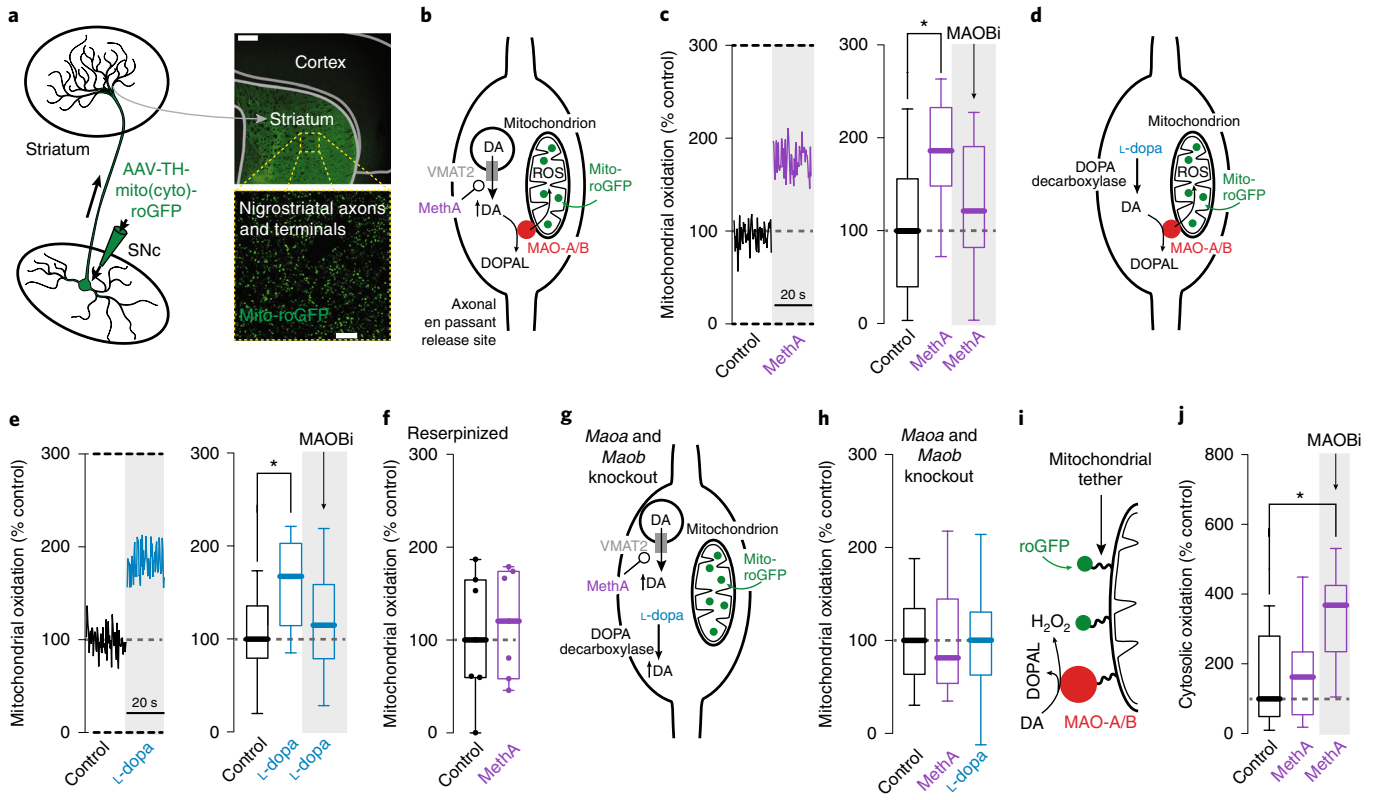

Fig. 1 | Mitochondrial thiol oxidation is increased by elevating cytosolic dopamine and prevented by inhibiting MAO enzymes in ex vivo brain slices. **a**, Left: cartoon depicting viral delivery of the redox-sensitive probe roGFP into dopaminergic neurons of the SNc. After viral delivery, the roGFP probe is expressed throughout dopaminergic neurons (soma, dendrites and axons). Right: sample images in the dorsolateral striatum showing roGFP (targeted to the mitochondrial matrix) expressed in dopaminergic axons; scale bars, 500 µm (top) and 10 µm (bottom). **b**, Cartoon depicting the actions of methamphetamine (MethA) on VMAT2 in axonal en passant release sites of dopaminergic neurons. ROS, reactive oxygen species. **c**, Methamphetamine increases mito-roGFP oxidation in dopaminergic axons. Left: sample traces illustrating methamphetamine-induced effects on mitochondrial redox compared to control. Right: perfusion of 10 µM methamphetamine ($n = 18$ slices from 9 mice) increases axonal mitochondrial oxidation relative to control ($n = 19$ slices from 10 mice) and is prevented by treatment with 10 µM rasagaline, an MAO-B inhibitor (MAOBi; $n = 18$ slices from 6 mice); Kruskal–Wallis test, $P = 0.0043$. Box-and-whisker plots depict the median, quartiles and range. **d**, Cartoon depicting L-dopa effects on cytosolic DA and mitochondrial redox in dopaminergic axonal en passant release sites. **e**, Addition of L-dopa (100 µM) increases mitochondrial oxidation in dopaminergic axons. Left: sample traces illustrating L-dopa-induced effects on mitochondrial redox compared to control. Right: similarly to methamphetamine, L-dopa ($n = 20$ slices from 6 mice) increases axonal mito-roGFP oxidation relative to control ($n = 14$ slices from 4 mice) and is prevented by MAO-B inhibitor; Kruskal–Wallis test, $P = 0.0001$. Box-and-whisker plots depict the median, quartiles and range. **f**, Methamphetamine (10 µM) has no effect on axonal mitochondrial oxidation in slices from mice depleted of DA by repeated in vivo administration of reserpine; $n = 7$ slices from 6 mice (two-sided Wilcoxon matched-pairs test, $P = 0.8048$). Box-and-whisker plots depict the median, quartiles and range. **g**, Cartoon illustrating the scenario for *Maoa* and *Maob* knockout. **h**, Neither methamphetamine (10 µM) nor L-dopa (100 µM) has an effect on axonal mitochondrial redox status in mice lacking both MAO-A and MAO-B: control, $n = 13$ slices from 3 mice; methamphetamine, $n = 11$ slices from 3 mice; L-dopa, $n = 13$ slices from 3 mice (Kruskal–Wallis test, $P = 0.6718$). Box-and-whisker plots depict the median, quartiles and range. **i**, Cartoon illustrating roGFP tethered to the outer mitochondrial membrane and the hypothesis that regional H_2O_2 production could result from MAO metabolism of DA. **j**, Methamphetamine (10 µM) has no effect on stress at the outer mitochondrial membrane, but stress is increased in the presence of MAO-B inhibitor: control, $n = 12$ slices from 3 mice; methamphetamine, $n = 10$ slices from 2 mice; methamphetamine + MAO-B inhibitor, $n = 11$ slices from 3 mice (Kruskal–Wallis test, $P = 0.0198$). Box-and-whisker plots depict the median, quartiles and range. *$P < 0.05$. Controls in **c**,**e**,**f**,**h**,**j**: bath perfusion of artificial cerebrospinal fluid (aCSF).

To ensure that the actions of rasagiline and clorgyline were not a result of 'off-target' effects, these experiments were repeated in mice in which both *Maoa* and *Maob* had been deleted[9]. Elevating cytosolic DA had no effect on axonal mitochondrial redox status in dopaminergic neurons within brain slices from these double-knockout mice (Fig. 1g,h). An attempt to rescue MAO activity by expression of a mutant form of MAO-B lacking the mitochondrial tethering sequence in knockout dopaminergic neurons yielded an increase in cytosolic (Extended Data Fig. 1i), but not mitochondrial (Extended Data Fig. 2e), oxidant stress in response to release of DA from vesicular stores.

To determine whether DA metabolism by MAO at the outer mitochondrial membrane generates H_2O_2 that affects redox status in the nearby mitochondrial matrix but not in the cytosol, a variant of roGFP was generated with the mitochondrial tethering peptide sequence from the C terminus of MAO. This placed the redox sensor in close physical proximity to MAO in dopaminergic neurons (Extended Data Fig. 1c–e). Subsequent release of vesicular DA (by acute bath application of 10 µM methamphetamine) did not detectably increase thiol oxidant status at the surface of mitochondria unless MAO was inhibited (Fig. 1i,j). In this situation, auto-oxidation of DA leading to the generation of H_2O_2 is likely to be responsible for the roGFP signal at the mitochondrial surface.

To verify that the ability of cytosolic DA to increase matrix oxidation was not peculiar to mouse dopaminergic neurons, human dopaminergic neurons were differentiated from induced

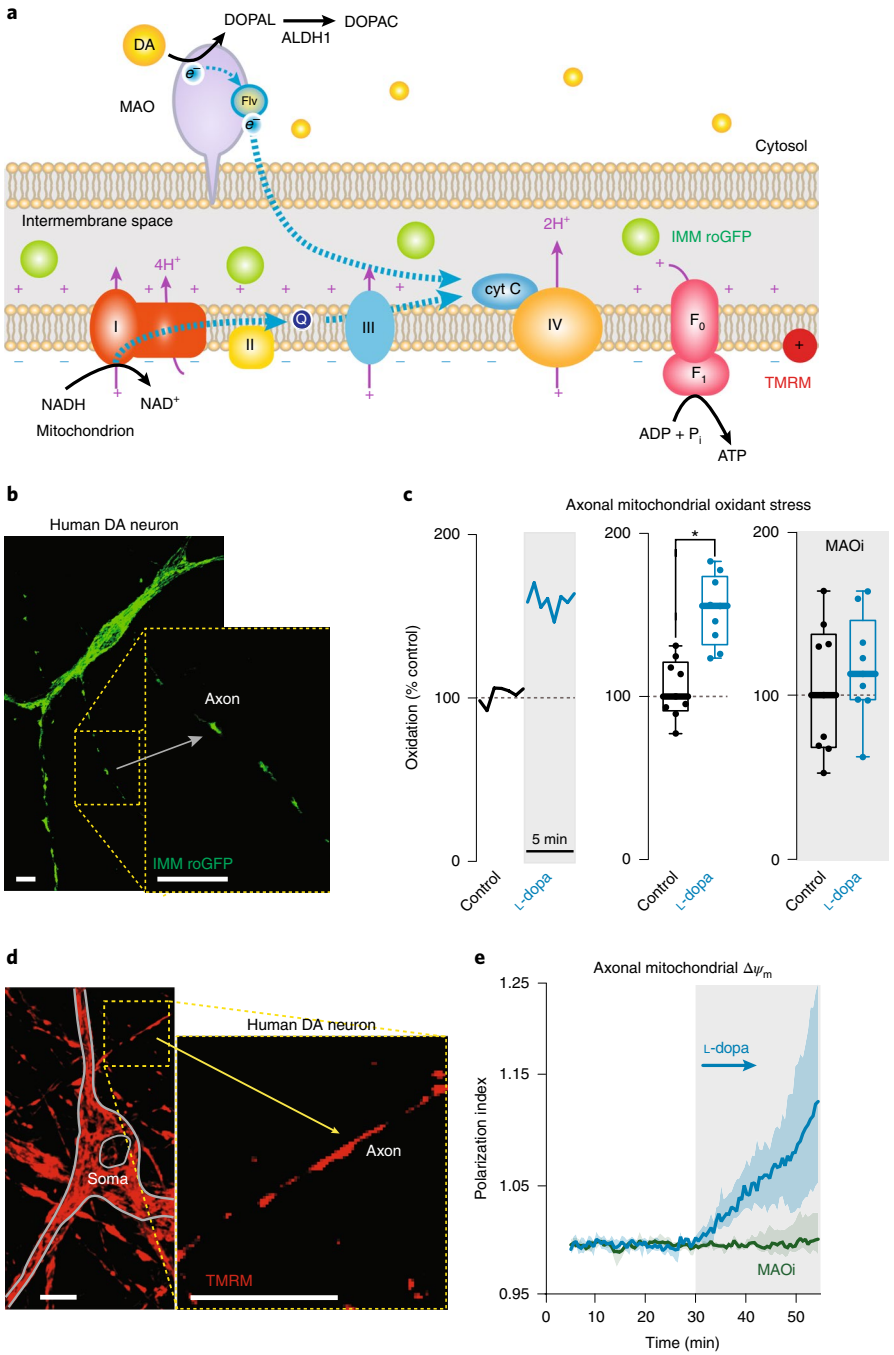

Fig. 2 | Elevating cytosolic dopamine with levodopa increases mitochondrial thiol oxidation by transferring electrons to the intermembrane space in human iPSC-derived dopaminergic neurons. a, Cartoon depicting the transfer of electrons from MAO metabolism of DA to the mitochondrial intermembrane space. IMM, inner mitochondrial membrane. **b**, Image of a DA-differentiated neuron expressing the redox-sensitive probe roGFP in the mitochondrial intermembrane space (left), and high-magnification image highlighting an axonal segment (right); scale bar, 10 µm. **c**, Left: sample traces illustrating the increase in intermembrane thiol oxidation induced by 100 µM L-dopa relative to control. Middle: L-dopa increases axonal oxidation in the intermembrane space compared to control; the experiment was performed using a within-subject design with repeated measures ($n = 9$ axons; two-sided Wilcoxon matched-pairs signed-rank test, $P = 0.0039$). Right: in a separate set of cells, L-dopa-induced oxidation is prevented by MAO inhibition with 5 µM clorgyline and 10 µM rasagiline; the experiment was performed using a within-subject design with repeated measures (MAOi, $n = 9$ axons; Wilcoxon matched-pairs signed-rank test, $P = 0.25$). Box-and-whisker plots depict the median, quartiles and range. **d**, Mitochondrial membrane potential was measured with TMRM to demonstrate the transfer of electrons to mitochondria by MAO metabolism of DA. A sample one-photon image of a DA-differentiated neuron loaded with TMRM dye (left) and a high-magnification image highlighting an axonal segment (right) are shown; scale bars, 10 µm. **e**, Addition of 2 µM myxothiazol to inhibit complex III and 1 µM carboxyatractyloside to inhibit adenine nucleotide translocase results in fluorescence decay of the TMRM signal. This decay was fit mathematically with a polynomial to characterize baseline decay (Extended Data Fig. 3). The observed data were normalized to the decay fit, generating a polarization index, with deviations from 1.0 indicating deviation from the fitting equation. Perfusion with 100 µm L-dopa ($n = 14$ axons) caused a significant deviation and was prevented by MAO inhibition ($n = 9$ axons); data are presented as median ± quartiles. $\Delta\psi_m$, change in mitochondrial membrane potential. Data were analyzed by comparison of fit of a quadratic, constrained to the time point of L-dopa administration ($P < 0.0001$). Controls were treated with aCSF.

Fig. 3 | Elevating cytosolic dopamine with levodopa increases ATP synthesis and is necessary for phasic dopamine release. a, An image of a DA-differentiated neuron expressing the ATP biosensor PercevalHR (left) and a high-magnification image highlighting an axonal segment (right); scale bars, 10 µm. **b**, Left: sample traces illustrating the increase in the ATP/ADP ratio induced by treatment with 100 µM L-dopa. Middle: L-dopa increases axonal ATP synthesis, measured as the ATP/ADP ratio, compared to control ($n=15$ axons; two-sided Wilcoxon matched-pairs signed-rank test, L-dopa-induced ATP synthesis is prevented by MAO inhibition with 5 µM clorgyline and 10 µM rasagiline (MAOi, $n=15$ axons; two-sided Wilcoxon matched-pairs signed-rank test, $P=0.0554$); the experiments were performed using a within-subject design with repeated measures. Box-and-whisker plots depict the median, quartiles and range. **c**, The ATP biosensor PercevalHR is expressed throughout dopaminergic neurons, as evidenced by sample images in the dorsolateral striatum; a low-magnification image (top; scale bar, 500 µm) and a high-magnification image (bottom; scale bar, 10 µm) illustrate striatal expression of PercevalHR in SNc dopaminergic axons. **d**, Left: L-dopa increases axonal ATP synthesis, measured as the ATP/ADP ratio, in SNc axons in the dorsolateral striatum compared to controls ($n=8$ slices from 3 mice; two-sided Wilcoxon matched-pairs signed-rank test, $P=0.0078$). Right: in a separate set of ex vivo slices, L-dopa-induced ATP synthesis is prevented by MAO inhibition with 10 µM rasagiline ($n=9$ slices from 2 mice; two-sided Wilcoxon matched-pairs signed-rank test, $P=0.2031$); the experiment was performed using a within-subject design with repeated measures. Box-and-whisker plots depict the median, quartiles and range. **e**, Cartoon illustrating the bioenergetically demanding process of DA release, reuptake and packaging into vesicles. **f**, Electrical stimulation trains (0.1 Hz) were used to deplete axonal ATP. Repeated measurements were taken at 950 nm and are presented as $\Delta F/F_0$; repetitive stimulation decreased axonal ATP. In the presence of the MAO-B inhibitor rasagiline, ATP levels were further decreased, and levels were yet further diminished with complex V inhibition (oligomycin) (lines are median values, and shading represents the interquartile range; control, $n=8$; MAO-B inhibitor, $n=9$; oligomycin, $n=6$ brain slices). **g**, To better visualize the contribution of MAO-B to ATP generation, the measurements in the presence of rasagaline were subtracted from those in control aCSF to yield MAO-B-dependent ATP (the line represents the median MAO-B/aCSF differential and shading corresponds to the interquartile range; $n=9$ brain slices). **h**, Pre-train: inhibition of MAO-B and complex V (oligomycin) both decreased the ATP/ADP bioenergetic index (Kruskal–Wallis test: aCSF versus rasagaline, $P=0.011$; aCSF versus oligomycin, $P=0.0005$; control, $n=7$; MAO-B inhibitor, $n=7$; oligomycin, $n=6$ brain slices). Post-train: electrical stimulation trains decreased ATP signal in all cases, but the effect was more pronounced in the absence of mitochondrial ATP production (Kruskal–Wallis test: aCSF versus oligomycin, $P=0.0005$; control, $n=6$; MAO-B inhibitor, $n=6$; oligomycin, $n=6$ brain slices). Box-and-whisker plots depict the median, quartiles and range. **i**, Images of dopaminergic axons expressing the DA biosensor dLight1.3b before and after electrical stimulation (1 pulse, 350 µA, 2 ms); scale bar, 10 µm. **j**, The release probability was interrogated using electrical stimulation to mimic tonic (1 pulse, 350 µA, 2 ms) or phasic (5 pulses, 350 mA, 2 ms, 100 Hz) DA release in the presence of synaptic blockade (10 µM mecamylamine and 10 µM sulpiride). Traces are shown of quantified dLight fluorescence in response to tonic or phasic release stimulation. The line shows the median and shading corresponds to the 95% confidence interval; control, $n=5$; MAO-B inhibitor, $n=6$; oligomycin, $n=4$ brain slices. **k**, No statistically significant difference was seen in tonic firing in response to MAO-B inhibitor (rasagaline, 10 mM) or oligomycin (10 mM). Phasic firing was significantly decreased by MAO-B inhibitor and was further decreased by oligomycin (two-way ANOVA, 5 pulses, 100 Hz: control versus rasagaline, $P=0.015$; control versus oligomycin, $P P=0.028$; control, $n=5$; MAO-B inhibitor, $n=6$; oligomycin, $n=4$ brain slices). Stimulation increased release ($F=169.63$, degrees of freedom (DFd) $=12$, $P F=10.07$, DFd $=12$, $P=0.003$) and altered stimulus response ($F=5.64$, DFd $=12$, $P=0.019$). Box-and-whisker plots depict the median, quartiles and range. $^*P<0.05$. Controls in all panels were treated with aCSF.

pluripotent stem cells (iPSCs). Increasing DA synthesis by acute exposure to L-dopa increased mitochondrial matrix roGFP oxidation in human dopaminergic neurons in a MAO-dependent manner, demonstrating the generality of the phenomenon (Extended Data Fig. 2f).

Where do the electrons generated from metabloism of DA by mitochondrially tethered MAO go? Mitochondria are biosynthetic 'engines' that use reducing equivalents to drive proton pumping by the ETC, creating an electrochemical gradient across the inner mitochondrial membrane. This gradient is used by complex V to convert ADP to ATP. For the electrons generated by MAO to reach the ETC, they would have to traverse the intermembrane space. This is plausible given that MAO binds flavin adenine dinucleotide, which can act as an electron shuttle, and many of the proteins that reside within the intermembrane space are capable of shuttling electrons[10] (Fig. 2a). To test the hypothesis that MAO activity increases the flux of electrons through the intermembrane space, a roGFP expression construct with an intermembrane space targeting sequence[11] was introduced into human dopaminergic neurons. After allowing expression of the protein (Fig. 2b), neurons were exposed to L-dopa for approximately 30 min to boost DA synthesis. This acute exposure to L-dopa robustly increased oxidation of roGFP within the intermembrane space in a MAO-dependent manner (Fig. 2c).

If MAO-derived electrons are shuttled to complex IV, then MAO activity should increase proton pumping and contribute to maintenance of the inner mitochondrial membrane potential. To test this hypothesis, the cationic dye tetramethylrhodamine (TMRM) was used to monitor inner mitochondrial membrane potential (Fig. 2d). Complex III was inhibited to block electron flux from earlier ETC complexes, and adenine nucleotide translocase was inhibited to prevent cytosolic ATP from driving complex V in reverse. As expected, inhibition of complex III and adenine nucleotide translocase caused TMRM fluorescence to decrease, confirming that inhibition of the ETC and complex V dissipates the inner mitochondrial membrane potential. The trajectory of the decrease was fit mathematically (Extended Data Fig. 3). In agreement with the proposition that MAO metabolism of DA was contributing to complex IV activity, boosting cytosolic DA levels consistently slowed the decline in TMRM fluorescence (Fig. 2e).

What are the functional consequences of MAO-catalyzed electron shuttling to the mitochondria? If electrons are shuttled to the ETC, then MAO activity could increase mitochondrial ATP production. To test this, the cytosolic ATP/ADP ratio was monitored using PercevalHR[12]. In human (Fig. 3a,b) and mouse (Fig. 3c,d) dopaminergic axons, acutely increasing cytosolic DA increased the ATP/ADP ratio in a MAO-dependent manner. Using repetitive electrical stimulation to emulate sustained neuronal activity, it was revealed that inhibiting MAO-B activity diminished cytosolic ATP levels, although not as profoundly as treatment with the complex V inhibitor oligomycin (10 µM) (Fig. 3e–h). However, the contribution of MAO-B to mitochondrial ATP production was transient, manifesting itself at the beginning of the stimulus train but not later (Fig. 3g,h). Because the affinity of VMAT2 for DA is several hundred fold greater than that of MAO-B[13,14], our interpretation of this result is that, as cytosolic DA falls with repetitive stimulation, VMAT2 out-competes MAO-B for DA, diminishing the effect of MAO-B metabolism on mitochondrial ATP generation.

Taken together, these observations suggest that, when cytosolic DA is abundant, electrons generated by MAO-B deamination of DA help axonal mitochondria meet the bioenergetic needs associated with transmitter release. To test this hypothesis, DA release was monitored using the genetically encoded optical sensor dLight (Fig. 3i)[15]. DA release was evoked with either a single electrical pulse or a five-pulse burst (100 Hz). Interestingly, DA release in response

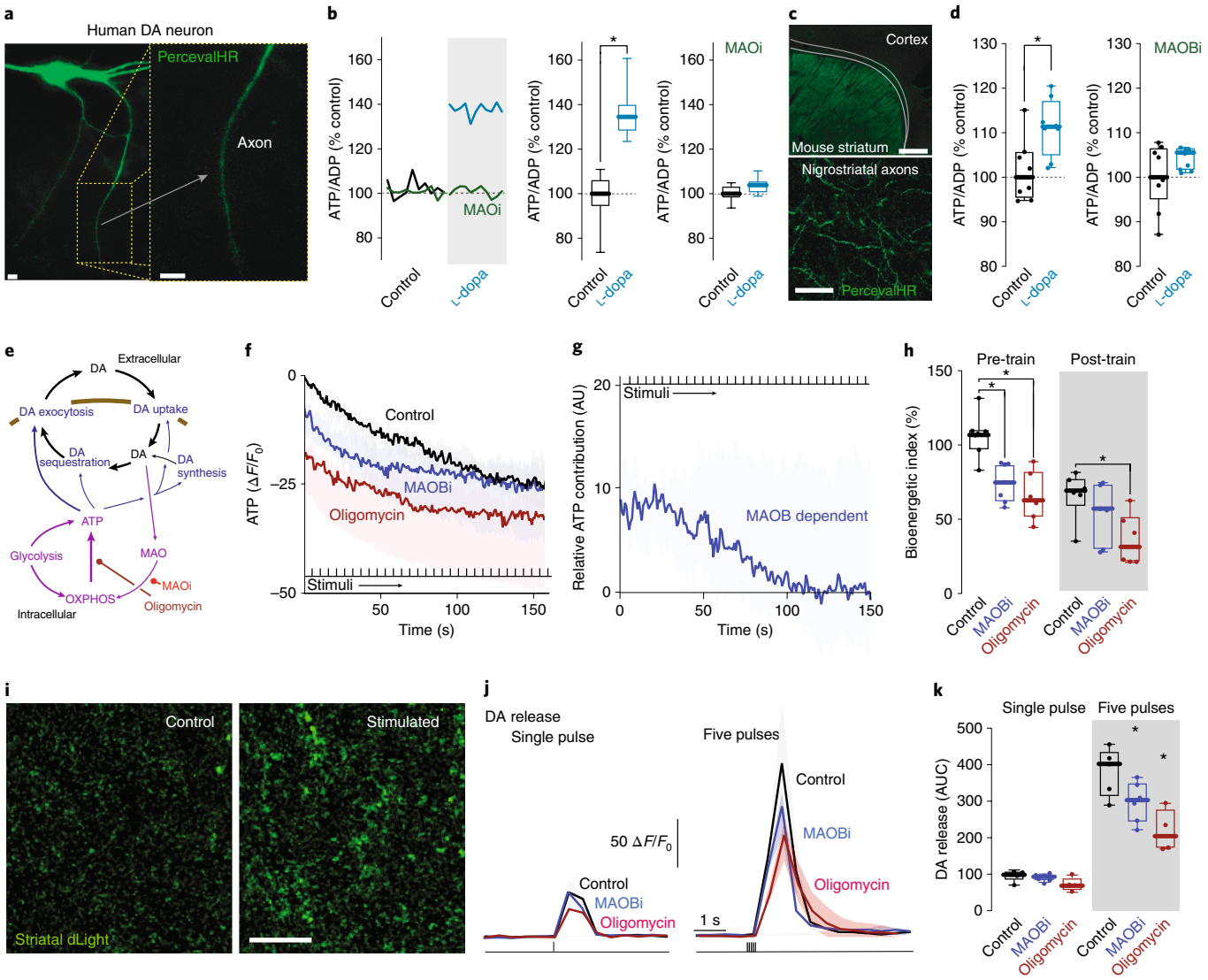

to a single stimulus was not affected by either MAO-B inhibition or oligomycin (Fig. 3j,k). This lack of mitochondrial dependence is consistent with recent work in glutamatergic neurons showing that glycolysis is capable of providing the energy necessary for a single release event[16]. However, as in other neurons[16], DA release in response to a short train of stimuli was dependent on mitochondrial ATP production and MAO-B (Fig. 3j,k); similar results were obtained using cyclic voltammetry to measure DA release (Extended Data Fig. 4). Thus, axonal MAO-B metabolism contributed to the bioenergetic requirements for sustained DA release.

MAO is thought to prevent neuronal oxidative stress by limiting quinone formation from DA, yet paradoxically, it also is thought to induce stress by generating H_2O_2 in the cytosol. Our findings challenge this view, revealing that electrons generated by MAO deamination of DA are shuttled to the ETC, contributing to inner membrane polarization and helping sustain DA release by increasing ATP production. This arrangement provides a biological rationale for the tethering of MAO to the outer mitochondrial membrane.

In vivo, the autonomous pacemaking of dopaminergic neurons is interrupted by bursts of spiking that convey environmental information and facilitate motor control[17–19]. During these bursts, DA reuptake could result in cytosolic DA accumulation. In these periods, MAO metabolism of DA could limit auto-oxidation but also could drive ATP generation to sustain the DA release needed to mobilize basal ganglia circuits and movement[20].

Online content

Any methods, additional references, Nature Research reporting summaries, source data, extended data, supplementary information, acknowledgements, peer review information; details of author contributions and competing interests; and statements of data and code availability are available at https://doi.org/10.1038/s41593-019-0556-3.

Received: 11 February 2019; Accepted: 12 November 2019;
Published online: 16 December 2019

References

1. Segura-Aguilar, J. et al. Protective and toxic roles of dopamine in Parkinson's disease. *J. Neurochem.* **129**, 898–915 (2014).
2. Fahn, S. & Cohen, G. The oxidant stress hypothesis in Parkinson's disease: evidence supporting it. *Ann. Neurol.* **32**, 804–812 (1992).
3. Kaludercic, N., Deshwal, S. & Di Lisa, F. Reactive oxygen species and redox compartmentalization. *Front. Physiol.* **5**, 285 (2014).
4. Dooley, C. T. et al. Imaging dynamic redox changes in mammalian cells with green fluorescent protein indicators. *J. Biol. Chem.* **279**, 22284–22293 (2004).
5. Sulzer, D., Sonders, M. S., Poulsen, N. W. & Galli, A. Mechanisms of neurotransmitter release by amphetamines: a review. *Prog. Neurobiol.* **75**, 406–433 (2005).
6. Mosharov, E. V., Gong, L. W., Khanna, B., Sulzer, D. & Lindau, M. Intracellular patch electrochemistry: regulation of cytosolic catecholamines in chromaffin cells. *J. Neurosci.* **23**, 5835–5845 (2003).

7. Mosharov, E. V. et al. Interplay between cytosolic dopamine, calcium, and α-synuclein causes selective death of substantia nigra neurons. *Neuron* **62**, 218–229 (2009).
8. Woodard, C. M. et al. iPSC-derived dopamine neurons reveal differences between monozygotic twins discordant for Parkinson's disease. *Cell Rep.* **9**, 1173–1182 (2014).
9. Chen, K., Holschneider, D. P., Wu, W., Rebrin, I. & Shih, J. C. A spontaneous point mutation produces monoamine oxidase A/B knock-out mice with greatly elevated monoamines and anxiety-like behavior. *J. Biol. Chem.* **279**, 39645–39652 (2004).
10. Brand, M. D. Mitochondrial generation of superoxide and hydrogen peroxide as the source of mitochondrial redox signaling. *Free Radic. Biol. Med* .**100**, 14–31 (2016).
11. Sabharwal, S. S., Waypa, G. B., Marks, J. D. & Schumacker, P. T. Peroxiredoxin-5 targeted to the mitochondrial intermembrane space attenuates hypoxia-induced reactive oxygen species signalling. *Biochem. J.* **456**, 337–346 (2013).
12. Tantama, M., Martinez-Francois, J. R., Mongeon, R. & Yellen, G. Imaging energy status in live cells with a fluorescent biosensor of the intracellular ATP-to-ADP ratio. *Nat. Commun.* **4**, 2550 (2013).
13. Youdim, M. B., Edmondson, D. & Tipton, K. F. The therapeutic potential of monoamine oxidase inhibitors. *Nat. Rev. Neurosci.* **7**, 295–309 (2006).
14. Wimalasena, K. Vesicular monoamine transporters: structure–function, pharmacology, and medicinal chemistry. *Med. Res. Rev.* **31**, 483–519 (2011).
15. Patriarchi, T. et al. Ultrafast neuronal imaging of dopamine dynamics with designed genetically encoded sensors. *Science* **360**, eaat4422 (2018).
16. Ashrafi, G. & Ryan, T. A. Glucose metabolism in nerve terminals. *Curr .Opin. Neurobiol.* **45**, 156–161 (2017).
17. Schultz, W. Multiple dopamine functions at different time courses. *Annu. Rev. Neurosci.* **30**, 259–288 (2007).
18. Schultz, W. Reward functions of the basal ganglia. *J. Neural. Transm.* **123**, 679–693 (2016).
19. Tsai, H. C. et al. Phasic firing in dopaminergic neurons is sufficient for behavioral conditioning. *Science* **324**, 1080–1084 (2009).
20. Gerfen, C. R. & Surmeier, D. J. Modulation of striatal projection systems by dopamine. *Annu. Rev. Neurosci.* **34**, 441–466 (2011).

Methods

Animals. Male mice expressing the redox-sensitive roGFP probe targeting the mitochondrial matrix under the tyrosine hydroxylase regulatory element[21], *Maoa* and *Maob* knockout mice[3], DAT bacTRAP mice[22] and wild-type mice (C57/Bl6) were bred in house and used with approval by the Northwestern and Rockefeller University Animal Care and Use Committees and in accordance with the National Institutes of Health (NIH) Guide for the Care and Use of Laboratory Animals. Animals were group housed with food and water provided ad libitum on a 12-h light/dark cycle and killed when between 5 and 10 weeks of age for all experiments, with the exception of DAT bacTRAP mice used for sequencing, which were killed at 4 months of age.

Stereotaxic surgery. PCR-amplified sequences for roGFP, mito-roGFP, truncated MAO-B lacking the C-terminal tail sequence required for anchoring (amino acids 492–520), PercevalHR (Addgene plasmid 49082)[12] and roGFP with the C-terminal anchoring sequence of MAO-B were subcloned into EcoRI and SalI restriction sites of the pFB-TH-SV40 vector and packaged into recombinant adeno-associated viruses (rAAVs) using serotype 9 with titers of 2.1×10^{13} viral genome copies per ml (Virovek). Mice were anesthetized using an isoflurane precision vaporizer (Smiths Medical) and placed in a stereotaxic frame (David Kopf Instruments) with a Cunningham adaptor (Harvard Apparatus) to maintain anesthesia delivery throughout surgery. After exposing the skull, a small hole was drilled and 350 nl of viral vector was delivered via a glass micropipette (Drummond Scientific) pulled on a Sutter P-97 puller. The SNc was targeted at the following coordinates: AP: −3.05, ML: 1.20 and DV: −4.30. All surgeries were performed in wild-type or *Maoa* or *Maob* knockout mice. Experiments in animals with stereotaxic delivery of AAV viral vectors were performed after at least ten postoperative days.

Ex vivo slice preparation. Mice were terminally anesthetized with a mixture of ketamine (50 mg kg^{-1}) and xylazine (4.5 mg kg^{-1}) and transcardially perfused with ice-cold modified aCSF containing 124.0 mM NaCl, 3.0 mM KCl, 1.0 mM $CaCl_2$, 2.0 mM $MgCl_2$, 26 mM $NaHCO_3$, 1.0 mM NaH_2PO_4 and 16.66 mM glucose. Once mice were perfused, the brain was rapidly removed and either sagittal or coronal slices containing the dorsolateral striatum (275 µm thick) or the SNc (220 µm thick) were sectioned using a vibratome (VT1200S, Leica Microsystems). Slices were transferred to a holding chamber containing normal aCSF with 124.0 mM NaCl, 3.0 mM KCl, 2.0 mM $CaCl_2$, 1.0 mM $MgCl_2$, 26 mM $NaHCO_3$, 1.0 mM NaH_2PO_4 and 16.66 mM glucose and allowed at least 30–40 min to recover before experiments. All solutions were pH 7.4 and 310–320 mOsm and were continually bubbled with 95% O_2 and 5% CO_2. Drugs (i.e., methamphetamine and L-dopa) used in ex vivo slice experiments were administered by acute bath application; the duration of application (methamphetamine, 10–20 min; L-dopa, >30 min) was far shorter than the duration needed to elicit degeneration, which requires >24 h of exposure.

Ex vivo redox and ATP measurements. Oxidant stress was assessed using redox-sensitive roGFP probe targeted to the cytosol, the outer mitochondrial membrane or the mitochondrial matrix, as previously described[11]. Slices were transferred to a recording chamber and continuously perfused with normal aCSF at 32–34 °C. Fluorescence was measured using an Ultima Laser Scanning Microscope system (Bruker) with a DODT contrast detector to provide bright-field transmission images with an Olympus ×60/0.9 NA lens. A two-photon laser (Chameleon Ultra II, Coherent) tuned to 920 nm was used to excite roGFP. Time series images of the roGFP probe were acquired with 60 frames obtained over ~20 s, with 0.195 µm × 0.195 µm pixels and 10- to 12-µs dwell times. The dynamic range of the probe was determined with 2 mM dithiothreitol, a reducing agent, and 200 µM aldrithiol, an oxidizing agent, which were used to sequentially perfuse slices, and time series images were acquired with each to determine the maximal and minimal fluorescence intensity. Test measurements were calculated as relative oxidation. Time series images were analyzed offline, and fluorescence measurements in multiple regions of interest were evaluated with the background subtracted[21]. ATP/ADP ratios were measured using the biosensor PercevalHR[12]. Time series images of the ATP biosensor were acquired as for roGFP experiments but were obtained over ~10 s with aCSF containing 3.5 mM glucose and slices perfused with 10 mM KCl or electrical stimulation (350 µA, 2 ms) to evoke activity. Two time series were obtained for each measurement, one with an excitation wavelength of 950 nm corresponding to ATP and a second at 820 nm corresponding to ADP[12]. ATP and ADP fluorescence was analyzed offline and quantified as the ATP/ADP ratio. Ratiometric measurement was not possible during application of the electrical stimulation trains. As such, 950-nm excitation was used to measure ATP binding to the probe. All final data are presented as the percentage of control (aCSF perfusion) and were normalized to the minimum ratio measured with non-hydrolyzable 2-deoxyglucose.

Human iPSC culture and neural differentiation. The iPSC line was generated from skin fibroblasts of a healthy individual through retroviral expression of OCT4, SOX2, c-MYC and KLF4 and was previously clinically characterized[23,24]. Differentiation of iPSCs into midbrain dopaminergic neurons was done according to published protocols, resulting in ~70% of cells expressing tyrosine hydroxylase with an array of dendritic and axonal processes[25]. To help control neuralization variability, cells were passaged en bloc (size, 1–2 mm) between days 11 and 14, followed by plating onto poly(*D*-lysine) (PDL)- and laminin-coated 10-cm dishes. Between days 25 and 30, neural blocks were passaged by accutase treatment onto PDL- and laminin-coated culture dishes. Neuralization growth factors were withdrawn at day 40, and neurons were maintained in Neurobasal medium (Life Technologies) containing Neurocult SM1 (Stemcell Technologies).

Redox, ATP and mitochondrial membrane potential measurements in iPSC-derived dopaminergic neurons. Human iPSC-derived dopaminergic neurons were grown on 12-mm glass coverslips and imaged between 75 and 88 d after differentiation. Two to 4 d before experimentation, dopaminergic neurons were infected with viral vectors targeting roGFP expression to the mitochondrial matrix (AAV9-TH-mito-roGFP), the mitochondrial intermembrane space (AAV9-TH-IMS-roGFP)[11] or the cytosol (AAV9-TH-cyto-roGFP)[26]. Cultures were transferred to an imaging chamber mounted on an inverted epifluorescence microscope (Nikon TE300) with a ×40/1.35NA oil-immersion objective. The imaging chamber was superfused with aCSF at a flow rate of 1 ml min^{-1}. Imaging experiments were carried out at 31–33 °C. Cells were illuminated by Polychrome V (TILL Photonics), and emissions were captured with a cooled CCD camera (Hamamatsu ImagEM) and Slidebook imaging software (Intelligent Imaging Innovations). Regions of interest in the dendrites or axon were selected for image analysis. For roGFP redox measurements, cells were exposed at two wavelengths (410 and 470 nm) sequentially for 50 ms each. Time-lapse ratiometric images (F410/F470) were captured every 30 s. Dopaminergic neurons expressing roGFP probes were imaged for 15 min to establish stable baselines; the perfusion buffer was then switched to aCSF containing 100 µM of L-dopa for 30 min or 10 µM rasagiline and 5 µM clorigyline for 30 min, followed by 100 µM L-dopa and 10 µM rasagiline and 5 µM clorigyline for 30 min. Afterwards, neurons were perfused with 2 mM dithiothreitol for 20 min and then with 100 µM aldrithiol for 20 min to obtain the full roGFP dynamic range[26].

For measurement of cytosolic ATP/ADP ratios, dopaminergic neurons expressing PercevalHR were excited at two wavelengths (420 and 490 nm) sequentially for 50 ms each; respective images were captured at 530 nm every 30 s. Cells were perfused with aCSF containing 3.5 mM glucose. After establishing stable baselines and treatment with 100 µM L-dopa for 30 min, with or without MAO inhibitors (10 µM rasagiline and 5 µM clorgyline), cells were perfused with aCSF containing 3.5 mM 2-deoxyglucose (replacing glucose) and 10 µM oligomycin to obtain the value of the minimum ATP/ADP ratio. All final data are presented as percentage of control (aCSF perfusion).

To monitor changes in mitochondrial membrane potential, dopaminergic neurons were loaded with 20 nM TMRM for 45 min, washed and maintained in 2 nM TMRM during imaging. Cells were exposed at 550 nm for 50 ms, and time-lapse images were captured every 30 s. After imaging for approximately 15 min to establish stable baselines, the complex III inhibitor myxothiazol (2 µM) and the adenine nucleotide translocase inhibitor carboxyatractyloside (1 µM) were added to the perfusion buffer for the remainder of the imaging. Thirty minutes later, cells were treated with 100 µM L-dopa, and imaging continued for an additional 30 min. To test MAO inhibition, 10 µM rasagiline and 5 µM clorgyline were added 30 min before addition of 100 µM L-dopa. Regions of interest with stable baseline fluorescence (less than 15% variation) were individually fit with centered, second-order polynomial regressions (average $r^2 > 0.90$ in all experiments), using data from the 30 min after complex III andANT inhibition (before L-dopa administration). The mitochondrial polarization index was calculated by dividing observed data by modeled data; deviation of polarization indices from 1.0 indicated deviation from the decay trajectory.

Dopamine release with dLight1.3b. Mice were stereotaxically injected with 350 nl of AAV.CAG.dLight1.3b in the SNc. Ten days after surgery, sagittal slices were prepared as previously described. Image series were taken via 2PLSM. DA release in response to electrical stimulation (350 µA, 2 ms, 1 pulse or 5 pulses at100Hz) was measured. Synaptic blockers (the nicotinic acetylcholine receptor antagonist mecamylamine and the D2 receptor antagonist sulpiride; 10 µM) were used to investigate release probability. ImageJ software was used to sum total pixel fluorescence, and from these data, $\Delta F/F_0$ and areas under the curve were calculated.

Dopamine release with fast-scan cyclic voltammetry. Custom-built carbon fiber microelectrodes (80–100 µm of exposed carbon fiber in silica) were inserted 100 µm into the dorsolateral striatum of coronal brain slices, opposite a pronged stimulation electrode. A cyclic waveform sufficient to oxidize and reduce DA (−0.3 to −1.4 V, 10 Hz, 400 V s^{-1}) was applied to the carbon fiber microelectrode (Dagan ChemCLAMP amplifier/headstage driven by Axon Digidata 1440A). DA release was elicited by electrical stimulation (single pulse, 350 µA, 2 ms) and measured as the current generated at the surface of the carbon fiber microelectrode. The normal stimulation frequency was every 4 min, which resulted in consistent and stable DA release. The stimulation frequency was increased to every 10 s, which resulted in DA release depletion, to assess the importance of MAO and mitochondrial ATP production to intense energy consumption.

TRAP analysis and RNA sequencing. Male hemizygous DAT bacTRAP mice[22] were randomly divided into groups of five mice. Brains were removed and sectioned using an ice-cold Adult Mouse Brain Slicer with 1-mm coronal slice intervals (Zivic Instruments). From the tissue section containing the midbrain, the SNc was dissected under a Nikon SMZ645 light microscope using a ×10 lens. Translated mRNAs were purified as described previously[27]. TRAP samples underwent DNase digestion using the RNase-Free DNase Set (Qiagen) and were subsequently purified with the RNeasy MinElute Cleanup Kit (Qiagen). Eluted RNA samples were analyzed on a 2100 Bioanalyzer (Agilent) using RNA Pico Chips (Agilent) to confirm RNA integrity, followed by measurement of RNA concentrations with the Quant-iT RiboGreen RNA Assay Kit (Life Technologies). cDNAs were prepared with the Ovation RNA-Seq System V2 kit (NuGEN), using an input of 1 ng of RNA. Next, 500 ng of cDNA from each sample was fragmented on a Covaris S2 Focused Ultrasonicator using the operating conditions recommended by the manufacturer for a target fragment size of 200 bp. Fragment size was confirmed on a 2100 Bioanalyzer using High Sensitivity DNA Chips (Agilent). Libraries for RNA sequencing were prepared with the TruSeq RNA Sample Preparation v2 kit (Illumina), starting the manufacturer's low-throughput protocol with the end repair step. The concentration of the RNA-seq libraries was determined on a 2100 Bioanalyzer using High Sensitivity DNA Chips. Subsequently, two libraries with different adaptors were multiplexed for sequencing. After confirming the concentration of the multiplexed samples on a 2100 Bioanalyzer using High Sensitivity DNA Chips, samples were analyzed on an Illumina HiSeq 2000 sequencer using 100-bp single-end sequencing. RNA-seq reads were mapped to the *Mus musculus* assembly 10 reference genome using TopHat version 2.0.11. FPKM values for all genes in each sample were calculated with Cufflinks version 2.2.1. To analyze differential gene expression between samples, DESeq version 1.14.0 was used under the standard comparison mode.

Statistical analysis. All data were analyzed in Prism (GraphPad Software). Datasets were not assumed to have normal distributions and thus were analyzed using non-parametric statistics. Data are presented as box-and-whisker plots depicting median, quartiles and range. Mann–Whitney tests (two-tailed), Wilcoxon matched-pairs signed-rank tests (two-tailed) and Kruskal–Wallis tests with Dunn's post hoc analysis were used where appropriate. For clarity, all data were normalized to respective controls and are presented as a percentage; $\alpha = 0.05$. Data collection and analysis were not performed with blinding to the conditions of the experiments. No statistical methods were used to predetermine sample sizes; sample sizes were determined on the basis of pilot studies, and randomization procedures were not used.

Reporting Summary. Further information on research design is available in the Nature Research Reporting Summary linked to this article.

Data availability

Data from this study are available from the corresponding author upon reasonable request.

Code availability

Analysis routines and code are available from the corresponding author upon reasonable request.

References

21. Guzman, J. N. et al. Oxidant stress evoked by pacemaking in dopaminergic neurons is attenuated by DJ-1. *Nature* **468**, 696–700 (2010).
22. Brichta, L. et al. Identification of neurodegenerative factors using translatome-regulatory network analysis. *Nat. Neurosci.* **18**, 1325–1333 (2015).
23. Mazzulli, J. R. et al. Gaucher disease glucocerebrosidase and α-synuclein form a bidirectional pathogenic loop in synucleinopathies. *Cell* **146**, 37–52 (2011).
24. Cooper, O. et al. Pharmacological rescue of mitochondrial deficits in iPSC-derived neural cells from patients with familial Parkinson's disease. *Sci. Transl. Med.* **4**, 141ra190 (2012).
25. Burbulla, L. F. et al. Dopamine oxidation mediates mitochondrial and lysosomal dysfunction in Parkinson's disease. *Science* **357**, 1255–1261 (2017).
26. Dryanovski, D. I. et al. Calcium entry and α-synuclein inclusions elevate dendritic mitochondrial oxidant stress in dopaminergic neurons. *J. Neurosci.* **33**, 10154–10164 (2013).
27. Heiman, M., Kulicke, R., Fenster, R. J., Greengard, P. & Heintz, N. Cell type-specific mRNA purification by translating ribosome affinity purification (TRAP). *Nat. Protoc.* **9**, 1282–1291 (2014).

Acknowledgements

This study was supported by grants from the JPB Foundation, the IDP Foundation, the Michael J. Fox Foundation and the NIH (NS047085) to D.J.S.; an NIH grant (NS076054) to D.K.; an NIH grant (DA039253) and a Northwestern Memorial Foundation grant to S.M.G.; the Boyd and Elsi Welin Professorship and Tsai Family Fund to J.C.S.; and NIH grants U01NS103522, U01NS090604 and DPMH107056 to L.T. The authors thank the Northwestern Center for Advanced Microscopy (supported by National Cancer Center Support Grant P30 CA060553) for assistance.

Author contributions

Conceptualization: D.J.S., S.M.G., K.A.S., P.T.S., Z.X. and D.K.; methodology: D.J.S., S.M.G., P.T.S., K.A.S. and Z.X.; investigation: S.M.G., K.A.S., Z.X., E.Z., L.F.B. and L.B.; formal analysis: S.M.G., K.A.S., Z.X. and L.B.; writing of the original draft: S.M.G. and D.J.S.; reviewing and editing: S.M.G., Z.X., E.Z., L.F.B., J.C.S., J.K., K.A.S., L.B., P.G., D.K., P.T.S. and D.J.S.; funding acquisition: S.M.G., D.K., P.G. and D.J.S.; resources: J.K., L.B., P.G., J.C.S., L.T. and T.P.; supervision: D.J.S.

Competing interests

The authors declare no competing interests.

Additional information

Extended data is available for this paper at https://doi.org/10.1038/s41593-019-0556-3.

Supplementary information is available for this paper at https://doi.org/10.1038/s41593-019-0556-3.

Correspondence and requests for materials should be addressed to D.J.S.

Peer review information *Nature Neuroscience* thanks Elizabeth Jonas and the other, anonymous, reviewer(s) for their contribution to the peer review of this work.

Reprints and permissions information is available at www.nature.com/reprints.

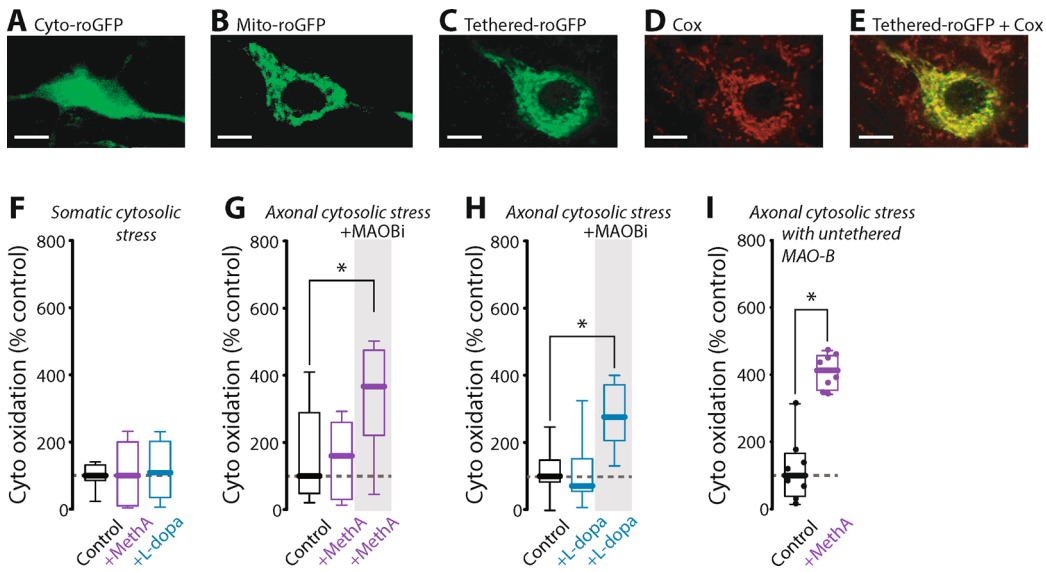

Extended Data Fig. 1 | Cytosolic thiol oxidation. The redox sensitive probe roGFP was targeted to the various cellular compartments compartment of substantia nigra pars compacta dopamine neurons for experiments throughout the manuscript. **a**, Sample image illustrating the expression pattern of cyto-roGFP. **b**, Sample image illustrating the expression pattern of Mito-roGFP; note the pattern of the mitochondrial matrix and absence of nuclear localization. **c**, Sample image illustrating the expression pattern of roGFP with a targeting sequence localizing the probe to the outter membrane of the mitochondria (same targeting sequence used by monoamine oxidase enzymes); the tethered roGFP presents a similar pattern of distribution of Mito-roGFP suggesting mitochondrial localization. **d**, Cytochrome c oxidase (Cox) counterstain of the same cell depicted in panel c. **e**, Merged image of the tethered-roGFP and Cox counterstain demonstrating colocalizaton. Scale bars denote 20 µm. dopaminergic neurons and levels of oxidant status were measured. **f**, Somatic cytosolic oxidation was unaltered by 10 µM methamphetamine (+MethA; n = 10 cells/3 mice) or 100 µM levodopa (+L-dopa; n = 11 cells/3 mice); control n = 11 cells/2 mice; Kruskal-Wallis test; $p = 0.9154$. Box-and-whisker plots depict median, quartiles, and range. **g**,+MethA (n = 11 slices/4 mice) had no effect on cytosolic oxidation in axons unless slices were incubated with 10 µM of the monoamine oxidase inhibitor rasagiline (+MAOBi; n = 10 slices/4 mice); control n = 11 slices/3 mice (Kruskal-Wallis test; $p = 0.0108$). Box-and-whisker plots depict median, quartiles, and range. **h**,+L-dopa (n = 13 slices/4mice) had no effect on axonal cytosolic oxidation unless in the presence of 10uM+MAOBi (n = 14 slices/4 mice); control n = 10 slices/3mice (Kruskal-Wallis test; $p < 0.001$). Box-and-whisker plots depict median, quartiles, and range. **i**, Monoamine oxidase knockout mice were stereotaxically delivered a variant of MAO-B lacking the tethering sequence targeting it to the outer membrane of the mitochondria and tested for methamphetamine (+Meth; 10 µM)-induced cytosolic thiol oxidation in axons. +Meth increased cytosolic oxidation in slices from mice expressing untethered MAO-B; n = 8 slices/3 mice (Wilcoxon matched-pairs two-sided signed rank test, $p = 0.0078$). Box-and-whisker plots depict median, quartiles, and range. *$p < 0.05$.

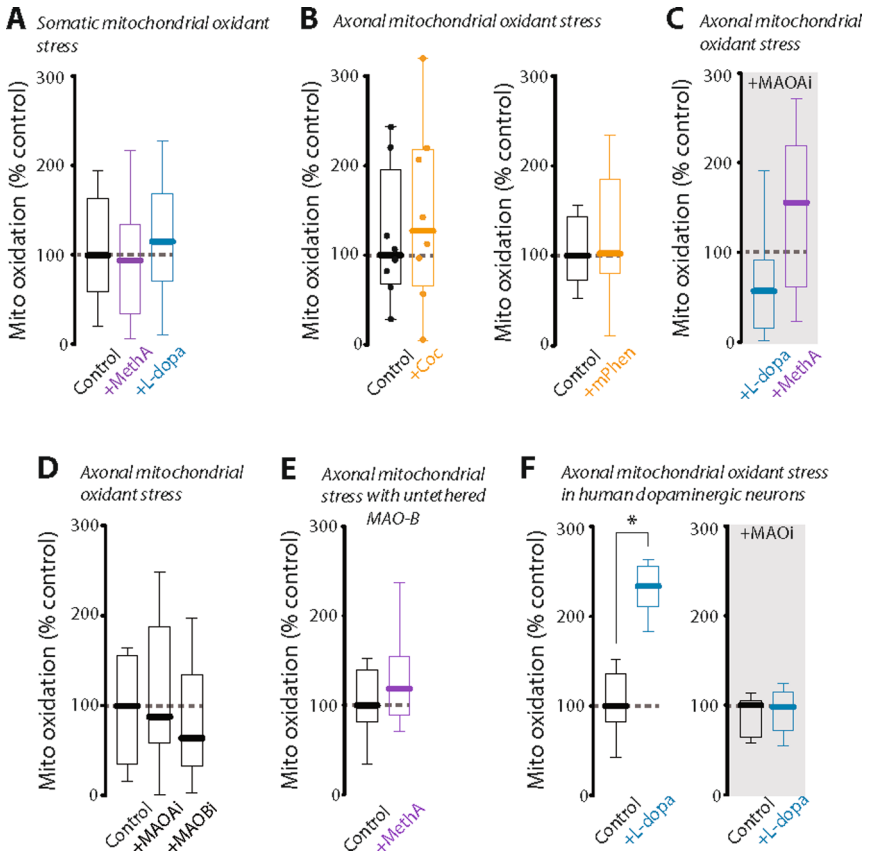

Extended Data Fig. 2 | Mitochondrial thiol oxidation. The redox sensitive probe roGFP was targeted to the mitochondrial matrix of substantia nigra pars compacta dopaminergic neurons and levels of thiol redox status were measured. **a**, Somatic Mito-roGFP oxidation was unchanged by treatments; control (n = 11 cells/6 mice), 10 μM methamphetamine (+MethA; n = 12 cells/4 mice), or 100 μM levodopa (+L-dopa; n = 18 cells/5 mice); Kruskal-Wallis test; p = 0.5341. Box-and-whisker plots depict median, quartiles, and range. **b**, Cocaine (left; 5 μM; +Coc) had no effect on mitochondrial thiol redox status in substantia nigra pars compacta dopaminergic axons (Wilcoxon matched-pairs signed rank test p = 0.6454; n = 8 slices/2 mice. Methylphenidate (right; 5 μM; +mPhen) also had no effect on axonal Mito-roGFP oxidation status (n = 11 slices/3 mice); Wilcoxon matched-pairs two-sided signed rank test; p = 0.4131. Box-and-whisker plots depict median, quartiles, and range. **c**, Clorgyline (5 μM; +MAOAi), a monoamine oxidase A inhibitor, prevented 100 μM levodopa (+L-dopa; n = 12 slices/3 mice; analyzed with Fig. 1e) and 10 μM methamphetamine (+MethA; n = 12 slices/4 mice; analyzed with Fig. 1b)-induced axonal Mito-roGFP oxidation. Box-and-whisker plots depict median, quartiles, and range. **d**, Monoamine oxidase inhibitors alone had no effect on axonal mitochondrial thiol redox status; control n = 10 slices/3 mice, +MAOAi n = 11 slices/3 mice, +MAOBi n = 11 slices/3 mice (Kruskal-Wallis test; p = 0.7413). Box-and-whisker plots depict median, quartiles, and range. **e**, Monoamine oxidase knockout mice were stereotaxically delivered a variant of MAO-B lacking the tethering sequence targeting it to the outer membrane of the mitochondria and tested for methamphetamine (+Meth; 10 μM)-induced mitochondrial thiol oxidation in axons. +Meth had no effect on mitochondrial oxidant staus in slices from mice expressing untethered MAO-B; n = 12 slices/3 mice (Wilcoxon matched-pairs two-sided signed rank test, p = 0.2036). Box-and-whisker plots depict median, quartiles, and range. **f**, Human iPSC-derived dopaminergic neurons were transfected with the redox sensitive probe roGFP targeted to the mitochondrial matrix. Basal levels of oxidant status were measured (control) followed by incubation with 100 μM levodopa (+L-dopa). +L-dopa increased axonal mitochondrial thiol oxidation; the experiment performed using a within-subject design with repeated measures (left; n = 15 axons; Wilcoxon matched-pairs two-sided signed rank test; $p < 0.0001$). In a separate set of cells monoamine oxidase inhibition (right) with 5 μM clorgyline +10 μM rasagiline (+MAOi) prevented+L-dopa-induced axonal mitochondrial thiol oxidation; experiment performed using a within-subject design with repeated measures; Wilcoxon matched-pairs two-sided signed rank test; p = 0.4973); n = 14 axons; box-and-whisker plots depict median, quartiles, and range. *$p < 0.05$.

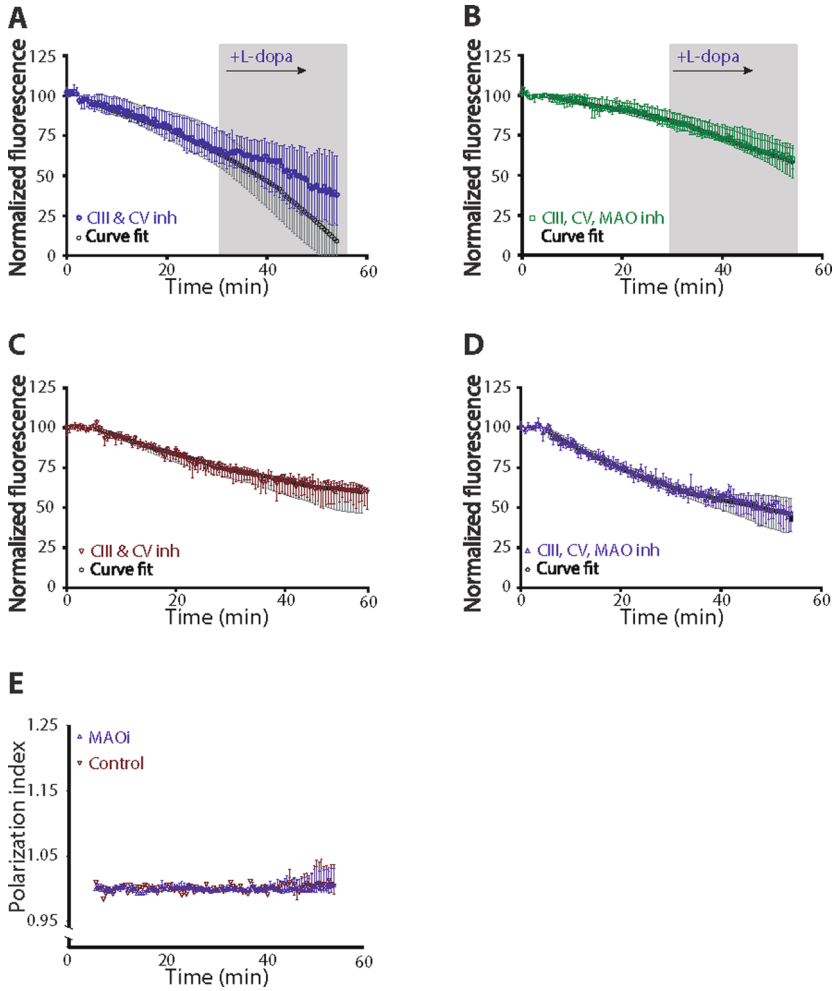

Extended Data Fig. 3 | Mitochondrial membrane potential measured by TMRM. a, An image of a dopamine (DA) differentiated neuron expressing the ATP biosensor Perceval HR (upper left) and high magnification highlighting an axonal segment (lower right); scale bars denote 10 µm. **b**, Sample traces (left) illustrating 100 µM levodopa (+L-dopa)-induced increase in ATP/ADP ratio. +L-dopa increased axonal ATP synthesis measured as ATP/ADP ratio compared to control (middle; n = 15 axons; Wilcoxon matched-pairs two-sided signed rank test; $p < 0.0001$). In a separate set of cells+L-dopa-induced ATP synthesis was prevented by MAO inhibition with 5 µM clorgyline+10 µM rasagiline (right; MAOi; n = 15 axons; Wilcoxon matched-pairs two-sided signed rank test; $p = 0.0554$); experiments performed using a within-subject design with repeated measures. Box-and-whisker plots depict median, quartiles, and range. **c**, The ATP biosensor Perceval HR expresses throughout dopaminergic neurons as evidenced by sample images in the dorsolateral striatum; low (upper left; scale bar denotes 500 µm) and high magnification images (lower right; scale bar denotes 10 µm) illustrating striatal expression of Perceval HR in SNc DA axons. **d**, +L-dopa increased axonal ATP synthesis measured as ATP/ADP ratio in SNc axons in the dorsolateral striatum compared to control (middle; n = 8 slices/3 mice; Wilcoxon matched-pairs two-sided signed rank test; $p = 0.0078$). In a separate set of *ex vivo* slices, +L-dopa-induced ATP synthesis was prevented by MAO inhibition with 10 µM rasagiline (right; +MAOBi; n = 9 slices/2 mice; Wilcoxon matched-pairs two-sided signed rank test; $p = 0.2031$); experiment performed using a within-subject design with repeated measures. Box-and-whisker plots depict median, quartiles, and range. **e**, Cartoon illustrating the bioenergetically demanding process of DA release, reuptake, and packaging into vesicles. **f**, Electrical stimulation trains (0.1 Hz) were used to deplete axonal ATP. Repeated measurements were taken at 950 nm and presented as $\Delta F/F_0$; repetitive stimulation decreased axonal ATP. In the presence of the MAO-B inhibitior rasagiline (+MAO-Bi) ATP levels were further decreased and yet further with complex V inhibition (+oligomycin) (lines are median values, shading is interquartile range; control n = 8, +MAOBi n = 9, and +oligomycin n = 6 brain slices). **g**, To better visualize the contribution of MAO-B to ATP generation, the measurements in the presence of rasagaline were subtracted from those in control aCSF to yield MAO-B dependent ATP (line represents the median MAO-B/aCSF differential, shading is interquartile range; n = 9 brain slices). **h**, *Pre-train:* Inhibition of MAO-B or complex V (+oligomycin) both decreased the ATP:ADP bioenergetic index (Kruskal-Wallis test: aCSF vs rasagaline $p = 0.011$, aCSF vs oligomycin $p = 0.0005$; control n = 7; +MAOBi n = 7; +oligomycin n = 6 brain slices). *Post-train:* Electrical stimulation trains decreased ATP signal in all cases but the effect was more pronounced in the absence of mitochondrial ATP production (Kruskal-Wallis test: aCSF vs oligomycin $p = 0.0005$, control n = 6; +MAOBi n = 6, +oligomycin n = 6). Box-and-whisker plots depict median, quartiles, and range **i**, Images of dopamine axons expressing dopamine biosensor dLight1.3b before and after electrical stimulation (1p, 350 µA, 2 ms); scale bar denotes 10 µM. **j**, Release probability was interrogated using electrical stimulation to mimic tonic (1p, 2 ms, 350 µA) or phasic dopamine release (5p100Hz, 2 ms, 350 uA) in the presence of synaptic blockade (10 µM mecamylamine, 10 µM sulpiride). Traces of quantified dLight fluorescence in response to tonic or phasic release stimulation. Line: median, shading 95% CI; control n = 5, +MAOBi n = 6, and +oligomycin n = 4 brain slices. **k**, No statistically significant difference was seen in tonic firing in response to +MAOBi (rasagaline, 10 uM) or +oligomycin (10 uM). Phasic firing was significantly decreased by +MAOBi and further decreased by +oligomycin (2-way ANOVA, 5p100Hz: control vs rasagaline $p = 0.015$, control vs oligomycin $p < 0.0001$, rasagaline vs oligomycin $p = 0.028$; control n = 5, +MAOBi n = 6, and +oligomycin n = 4 brain slices). Stimulation increases release ($F = 169.63$, $DFd = 12$, $p < 0.0001$). Drug affects release ($F = 10.07$, $DFd = 12$, $p = 0.003$. The drugs alter stimulus response ($F = 5.64$, $DFd = 12$, $p = 0.019$). Box-and-whisker plots depict median, quartiles, and range. *$p < 0.05$.

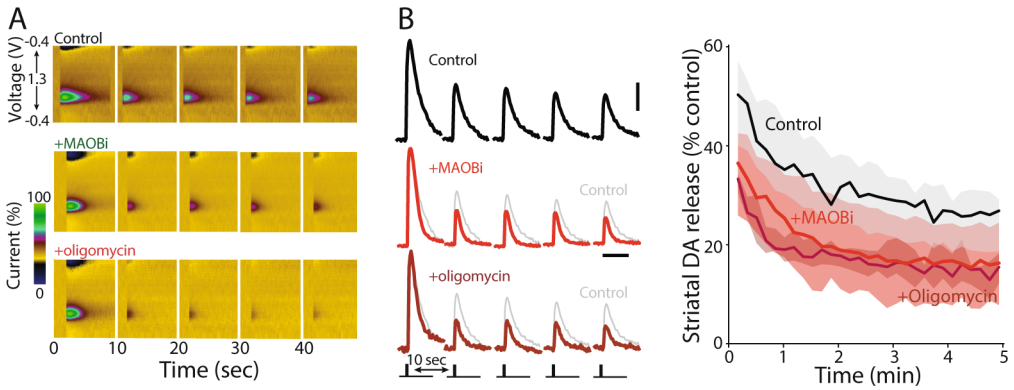

Extended Data Fig. 4 | MAO is necessary for maintaining phasic dopamine release. a, Sample color plots depicting the effects of MAO inhibition (10 μM rasagiline; +MAOBi) and ATP synthase inhibition with oligomycin (10 μM) on repeated DA release using fast scan cyclic voltammetry. **b**, Summary data of peak DA levels shows increased depletion when MAO and ATP synthesis are inhibited; vertical and horizongal scale bars denote 25% maximal release and 2.5 seconds, respectively. Data are normalized to the first peak of the stimulation train (line: median, shaded: 95% confidence interval, control n = 10, +MAOBi n = 6, and +oligomycin n = 7 brain slices, fit with one-phase decay with comparison of fit, $p < 0.001$).

nature research

Corresponding author(s): D. James Surmeier

Last updated by author(s): Oct 12, 2019

Reporting Summary

Nature Research wishes to improve the reproducibility of the work that we publish. This form provides structure for consistency and transparency in reporting. For further information on Nature Research policies, see Authors & Referees and the Editorial Policy Checklist.

Statistics

For all statistical analyses, confirm that the following items are present in the figure legend, table legend, main text, or Methods section.

n/a	Confirmed	
☐	☒	The exact sample size (*n*) for each experimental group/condition, given as a discrete number and unit of measurement
☐	☒	A statement on whether measurements were taken from distinct samples or whether the same sample was measured repeatedly
☐	☒	The statistical test(s) used AND whether they are one- or two-sided *Only common tests should be described solely by name; describe more complex techniques in the Methods section.*
☒	☐	A description of all covariates tested
☒	☐	A description of any assumptions or corrections, such as tests of normality and adjustment for multiple comparisons
☐	☒	A full description of the statistical parameters including central tendency (e.g. means) or other basic estimates (e.g. regression coefficient) AND variation (e.g. standard deviation) or associated estimates of uncertainty (e.g. confidence intervals)
☐	☒	For null hypothesis testing, the test statistic (e.g. *F*, *t*, *r*) with confidence intervals, effect sizes, degrees of freedom and *P* value noted *Give P values as exact values whenever suitable.*
☒	☐	For Bayesian analysis, information on the choice of priors and Markov chain Monte Carlo settings
☒	☐	For hierarchical and complex designs, identification of the appropriate level for tests and full reporting of outcomes
☒	☐	Estimates of effect sizes (e.g. Cohen's *d*, Pearson's *r*), indicating how they were calculated

Our web collection on statistics for biologists contains articles on many of the points above.

Software and code

Policy information about availability of computer code

Data collection	PrairieView, Wildcat, and Slidebook
Data analysis	Graphpad Prism, excel, ImageJ

For manuscripts utilizing custom algorithms or software that are central to the research but not yet described in published literature, software must be made available to editors/reviewers. We strongly encourage code deposition in a community repository (e.g. GitHub). See the Nature Research guidelines for submitting code & software for further information.

Data

Policy information about availability of data

All manuscripts must include a data availability statement. This statement should provide the following information, where applicable:

- Accession codes, unique identifiers, or web links for publicly available datasets
- A list of figures that have associated raw data
- A description of any restrictions on data availability

Data from this study are available from the corresponding author upon reasonable request.

Field-specific reporting

Please select the one below that is the best fit for your research. If you are not sure, read the appropriate sections before making your selection.

☒ Life sciences ☐ Behavioural & social sciences ☐ Ecological, evolutionary & environmental sciences

For a reference copy of the document with all sections, see nature.com/documents/nr-reporting-summary-flat.pdf

Life sciences study design

All studies must disclose on these points even when the disclosure is negative.

Sample size	A Gaussian distribution was not assumed. Moreover, small-moderate sample sizes (e.g. n<15) are prone to type I errors with normality tests. Most of the datasets in the current report are below the threshold for a reliable and meaningful normality test. Therefore, non-parametric statistics were used and as such a power analysis could not be conducted. This is the first study to explore oxidant stress in axonal compartments so there was no literature to determine appropriate sample sizes and degree of variability. Sample size were thus determined based on pilot studies conducted in the Surmeier lab.
Data exclusions	no data exclusions
Replication	The seminal finding (i.e. methamphetamine-induced increase in axonal mitochondrial stress) was independently reproduced by a graduate student and a post-doctoral fellow; this data is not included in the manuscript. Moreover, each experiment was performed multiple times across multiple mice as articulated in figure legends. All findings in this manuscript were replicated across animals/brain slices/ differentiated cells on separate coverslips and data pooled for analysis and presentation.
Randomization	Tissue used in studies were randomly assigned to experimental groups but a formal randomization procedure was not implemented.
Blinding	blinding was not used for data collection or analysis; scientific rigor is provided by using multiple models/systems to test our hypotheses (i.e. mouse tissue and human differentiated stem cells).

Reporting for specific materials, systems and methods

We require information from authors about some types of materials, experimental systems and methods used in many studies. Here, indicate whether each material, system or method listed is relevant to your study. If you are not sure if a list item applies to your research, read the appropriate section before selecting a response.

Materials & experimental systems

n/a	Involved in the study
☐	☒ Antibodies
☐	☒ Eukaryotic cell lines
☒	☐ Palaeontology
☐	☒ Animals and other organisms
☐	☒ Human research participants
☒	☐ Clinical data

Methods

n/a	Involved in the study
☒	☐ ChIP-seq
☒	☐ Flow cytometry
☒	☐ MRI-based neuroimaging

Antibodies

Antibodies used	Anti-OxPhos Complex IV Subunit I Monoclonal Antibody also called Cytochrome c oxidase (Invitrogen Life Technologies, Carlsbad, CA, USA) Cat#459600. PRID :AB_2532240Clone ID of monoclonal antibody 1D6E1A8. concentration 1mg/ml in Hepes-Buffered Saline. dilution 1:500 Alexa Fluor 546 Goat anti mouse (IgG) a second antibody (Invitogen) with 1:500 dilution. Cat # A-11030 RRID AB_2556548.
Validation	all antibodies used are commercially available and validated in existing literature and/or from manufacturer Reference for COX antibody: https://www.ncbi.nlm.nih.gov/pmc/articles/PMC3997697/

Eukaryotic cell lines

Policy information about cell lines

Cell line source(s)	iPSC cell line was generated from skin fibroblasts of a healthy individual as detailed in the methods section.
Authentication	The cell line was generated through retroviral expression (see methods for details) and previously clinically characterized (see methods and citations therein).
Mycoplasma contamination	Cell lines were not tested for mycoplasma contamination.
Commonly misidentified lines (See ICLAC register)	no commonly misidentified cell lines were used.

Animals and other organisms

Policy information about studies involving animals; ARRIVE guidelines recommended for reporting animal research

Laboratory animals	Male mice expressing roGFP in dopaminergic neurons (mitochondrially targeted; refer to reference in methods section), DAT-cre-Risp, monoamine oxidase A/B knockout, DAT bacTRAP, and wild-type C57/Bl6 mice were used and sacrificed at 5-10 weeks of age with the exception of DAT bacTRAP mice which were sacrificed at 4 months of age.
Wild animals	no wild animals were used
Field-collected samples	no field-collected samples were used
Ethics oversight	Northwestern and Rockefeller University Animal Care and Use Committees

Note that full information on the approval of the study protocol must also be provided in the manuscript.

Human research participants

Policy information about studies involving human research participants

Population characteristics	material from human subjects (skin fibroblasts) were used to differentiate into dopaminergic neurons; aside from this use of tissue, human subjects were not used.
Recruitment	*Describe how participants were recruited. Outline any potential self-selection bias or other biases that may be present and how these are likely to impact results.*
Ethics oversight	*Identify the organization(s) that approved the study protocol.*

Note that full information on the approval of the study protocol must also be provided in the manuscript.